

MECHANICAL EFFECTS AT HIGH HYDROSTATIC PRESSURE*

CH. HARTMANN, A. DELGADO

Chair of Fluidynamics and Process Control, TU München, Germany

e-mail: Christoph.Hartmann@wzw.tum.de, delgado@wzw.tum.de

Наличие высокого гидростатического давления (ВГД) приводит к нарушению равновесия образования химических связей в биохимических реакциях, фазовых переходах и процессах переноса. Таким образом, ВГД, как новый метод в науке о продуктах питания и биотехнологии, предлагает широкий спектр приложений. Данная работа на двух примерах иллюстрирует влияние механических эффектов на биотехнологические и биологические преобразования при применении высокого гидростатического давления. В первом случае исследованы макроскопические процессы переноса жидкости вследствие действия давления и их влияние на однородность полученных результатов процесса. Во втором примере рассмотрено давление как механическая нагрузка на одну дрожжевую клетку (*Saccharomyces cerevisiae*) и проиллюстрированы деформация и напряжения вследствие этой нагрузки. Обсуждается связь с другими исследованиями, описанными в литературе.

Introduction

The application of hydrostatic pressures up to 1000 MPa has manifold effects on biotic and abiotic matter such as solid-liquid phase transitions, the unfolding of proteins, the inactivation of enzymes as well as the preservation of aroma compounds and vitamins. Besides above mentioned effects, high hydrostatic pressure inactivates micro-organisms offering a food preservation technique which is much more sensitive with respect to the generic properties of food than thermal treatment.

Therefore, high hydrostatic pressure (HHP) processing is increasingly used in food technology and biotechnology. Current applications are pressure induced freezing and thawing, high pressure pasteurization, tenderizing of meat and preservation of fresh products. Further potential applications can be found in medical technology (cryo-conservation of organs) and bio-material science.

High Pressure Processing is carried out as a batch process, which means that the substance is placed in a high pressure chamber. Then, pressure transmitting liquid (which might be the product itself) is pumped through an inlet vane into the chamber. Since temperature is kept roughly constant, this increase of mass leads to an increase of density and, thus, pressure. After several seconds to minutes, the compression phase is terminated by stopping the inflow of liquid. Then, the pressure level is kept approximately constant for up to one hour giving the

*The authors acknowledge the support of DFG within the grant FOR 358.

© Институт вычислительных технологий Сибирского отделения Российской академии наук, 2004.

pressure induced conversions enough time to take place. Finally, the pressure level is reduced by decompression and the product is taken out of the chamber.

Current paper illustrates the influence of mechanical effects on biotechnological and biological transformations during HHP processing on two examples: The first one deals with macroscopic fluid transport processes induced by compression and heterogeneous temperature fields. Most pressure sensitive effects are also depending on temperature fields. Hence both, convective motion and exposure to heterogeneous thermal conditions might induce a non-uniformity in the process engendering product quality variations that are inadmissible especially in biotechnology where product safety is an important issue.

The second example considers pressure as a mechanical load on a single yeast cell (*Saccharomyces cerevisiae*) and illustrates deformation and stresses resulting from this load. It will be shown, that hydrostatic pressure induces non-hydrostatic stress states in the cell due to its structured composition. Mechanical damages reported in literature can be explained by this approach. A correlation to those investigations is found and discussed.

In both examples computational techniques are applied as method of investigation. This approach overcomes the difficulties related to experimental *in-situ* techniques [3, 4, 12] at high pressure conditions.

1. High Pressure Processing on the Macro-Scale: Assessment of Thermally Induced Process Non-uniformities

During High Hydrostatic Pressure (HHP) Processing, an increase of temperature during the compression phase can be observed due to partial conversion of mechanical work into thermal energy. Heat transport between the solid structure of the autoclave and its content leads to transient, spatially non-uniform temperature fields. The degree of thermal non-uniformity depends on the geometrical shape and size as well as on the material properties of the autoclave. Furthermore, the content of the autoclave plays an important role. It is directly related to the process non-uniformity since in most cases, the pressure sensitive conversion is also dependent on temperature.

In direct processing, heat transport occurs between the treated liquid and the surrounding solid structure of the autoclave [1]. In indirect processing, the packaging material as well as the pressure transmitting fluid influences significantly the temperature fields [2].

Time scales and temperature differences increase with the chamber volume, which makes making effects of non-uniformity more prominent in larger chambers. It is subject of current research in the group of the authors to design a high pressure autoclave (2 litres volume) with optical accessibility in order to apply optical fluid and temperature measurements. Presently, numerical techniques are the methods of choice in order to carry out scale-up analyses of the thermofluidynamics and its interaction with biotechnological conversions.

The pressure induced temperature increase can be deduced from the conservation equation for the specific total enthalpy H according to

$$\frac{\partial(\rho H)}{\partial t} + \nabla \cdot (\rho \vec{v} H) = \frac{\partial p}{\partial t} + \nabla \cdot (\lambda \nabla T) + \nabla \cdot (\tau \cdot \vec{v}) + \rho \vec{g} \cdot \vec{v}, \quad (1)$$

where \vec{v} represents the fluid velocity vector, \vec{g} the gravity vector, ρ the fluid density, p the pressure, t the time and τ the tensor of viscous stresses. Further use of the conservation equation

for the specific enthalpy h

$$\rho \frac{Dh}{Dt} - \frac{Dp}{Dt} = \nabla \cdot (\lambda \nabla T) + \eta \Phi + \rho \vec{g} \cdot \vec{v}, \quad (2)$$

with Φ representing the dissipation function, and use of the thermodynamic relationship

$$\frac{Dh}{Dt} = \left. \frac{\partial h}{\partial p} \right|_T \frac{Dp}{Dt} + \left. \frac{\partial h}{\partial T} \right|_p \frac{DT}{Dt} = \frac{1}{\rho} (1 - \alpha T) \frac{Dp}{Dt} + c_p \frac{DT}{Dt}, \quad (3)$$

where α is the thermal expansion coefficient, one obtains the equation of thermal energy

$$\rho c_p \frac{DT}{Dt} = \alpha T \frac{Dp}{Dt} + \nabla \cdot (\lambda \nabla T) + \eta \Phi + \rho \vec{g} \cdot \vec{v}. \quad (4)$$

Latter equation reveals that the material derivative of the temperature T with respect to time t is governed by the material derivative of the pressure p with respect to time t as long as dissipation function Φ and potential energy as well as conductive heat flux are low. In this case one can approximate the transport equation of thermal energy through

$$\frac{DT}{Dt} \approx \frac{\alpha T}{\rho c_p} \frac{Dp}{Dt}. \quad (5)$$

For example, water at room temperature exhibits an increase of temperature of 2.5 K to 3 K when compressed to 100 MPa. Doing the same experiment with edible oils or alcohols, the temperature increase might be 10 K and more. Starting from higher initial temperatures, the increase becomes even stronger. This mechanism together with heat transfer effects is responsible for the generation of heterogeneous temperature distributions, which, in turn, interact with the biotechnological conversion.

Fluid motion is necessarily involved in High pressure treatment of a liquid substance. In order to show this mathematically, it is assumed that the density increases with increasing pressure and decreases with increasing temperature, which is valid for the most food and food related substances at ambient conditions. The development of a flow field in a fluid initially at rest during compression can be shown most conveniently with the equation of mass balance

$$\frac{\partial \rho}{\partial t} + \nabla \cdot (\rho \vec{v}) = 0. \quad (6)$$

During the compression phase, the density increases with increasing pressure. Consequently, the first term of equation (6) becomes non-zero. Since the left hand side has to equal zero, the fluid velocity \vec{v} has to adopt non-zero values. Therefore, pressure increase enforces a fluid motion. Temperature gradients play an important role in the deviation of the flow behaviour from the hydrostatic state. This can be seen on the basic equations of hydrostatics

$$\frac{\partial p}{\partial x} = 0, \quad (7)$$

$$\frac{\partial p}{\partial y} = 0, \quad (8)$$

$$\frac{\partial p}{\partial z} = -\rho \vec{g}. \quad (9)$$

In equations (7, 8, 9) x , y and z are Cartesian coordinates. It is assumed without a loss of generality, that the gravity vector points in the negative z direction. Further derivation of equation (8) with respect to z and of equation (9) with respect to y yields

$$\frac{\partial^2 p}{\partial y \partial z} = \frac{\partial^2 p}{\partial z \partial y} = -\frac{\partial \rho}{\partial y} \vec{g}. \quad (10)$$

Consequently, the right hand side of (10) and thus the derivative of the density with respect to y has to be constant and equal to zero

$$\frac{\partial \rho}{\partial y} = 0. \quad (11)$$

In general, this condition as deduced from hydrostatics can not hold. As long as density is a function of temperature and latter is subject to transport in a direction different from that of the gravity vector, equation (11) is violated. Hence, a fluid flow with non-zero velocity must necessarily develop and leads to convective transport of heat and suspended substances.

1.1. Pressure Chamber and Process Conditions

Analyses are conducted for a high pressure chamber of type CIP 6000 (Alstom Nantes, France). A maximum operating pressure of 600 MPa can be achieved in the temperature range of 253 to 353 K. Its internal diameter is 120 mm and its inner height is 310 mm. It has an internal volume of 3.3 litres. Fig. 1 illustrates the geometry of the chamber.

Two channel openings at the bottom of the chamber are approximately 10 mm off the central axis. One of the channels serves as inflow channel while the other one is closed during normal operation. The inflow channel at the bottom has an internal diameter of 1.6 mm. Water is used as experimental fluid. The chamber is completely filled at the beginning. The considered process consists of a compression to an operating pressure of 500 MPa. Then, the pressure is preserved for 820 s before decompression starts at the same rates than compression. The temperature

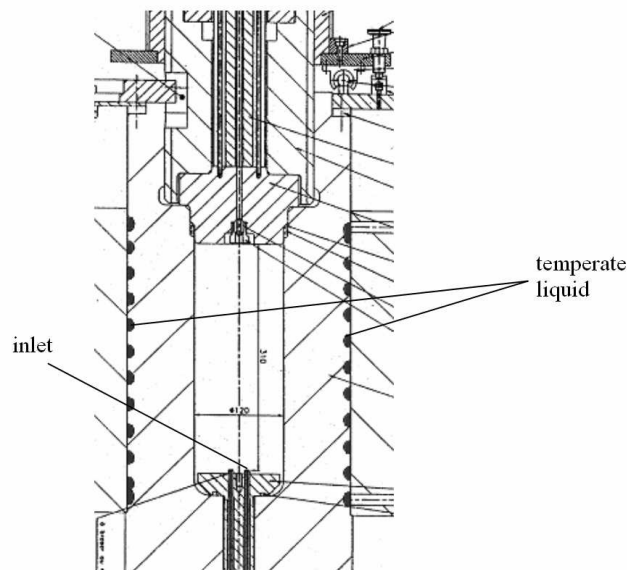


Fig. 1. A cross section through the geometry of the high-pressure chamber.

of the temperate liquid circulating in the cooling coil embedded in the solid structure of the chamber is controlled at 295 K.

In the current case, the effect of thermally induced non-uniformity is investigated for the example of a high pressure induced enzyme inactivation. The inactivation is assumed to obey the kinetics of *Bacillus subtilis* α -amylase dissolved in a 0.01 M Tris HCl buffer (pH 8.6) at a concentration of 15 g per litre. The substances are assumed to be ideally mixed at the beginning of the compression so that no concentration gradients existed. This inactivation process is a representative model process for many high pressure induced conversions.

The inactivation of *Bacillus subtilis* α -amylase obeys a first order kinetics [5]. Thus, the temporal and spatial distribution of the activity can be described by the equation

$$\frac{\partial(\rho A)}{\partial t} + \nabla \cdot [\rho A \vec{v}] = -\rho K(p, T)A, \quad (12)$$

where the relative activity A (actual activity related to the initial activity) can vary between 100% and values close to zero. The inactivation rate constant (K) depends on temperature and pressure and has been determined for both static and dynamic thermal and pressure conditions [8]. The left hand side contains the coupling between A and the flow field, i. e. the velocity of the solution. The right hand side represents the coupling of A and the temperature distribution. Furthermore, the fluid velocity field is coupled again with the temperature field due to compressibility and buoyancy effects. The activity throughout the whole chamber is initially 100%. During compression new fluid with enzyme of 100% activity flows into the chamber at 0.25 m/s. The initial and inflow temperature are set at to 313 K in order to achieve an inactivation effect at pressures of 500 MPa.

1.2. Numerical Methods

The conservation equations of mass, momentum and total energy, completed by a transport equation accounting for transport of the enzyme represented by its activity have to be solved, taking into account non-stationarity and compressibility of the fluid.

An equation of state accounting for the compressibility of pure water under high pressures up to 2500 MPa is implemented in the code in order to describe the density as a function of pressure and temperature. The equation of state is taken from [10]. The dependency of the specific heat from pressure and temperature has been taken from the same publication. The dependency of the viscosity on pressure and temperature is based on [11–13]. The implemented model is valid up to 600 MPa and up to 423 K.

The governing equations are solved with the finite volume method. A commercial software ANSYS CFX-4.4TM is used for convenience, enhanced by own software routines covering more than 5.000 statements of FORTRAN 90 code. The computations are carried out on a workstation and last about 15h.

The geometry of the HP chamber is not axisymmetric since the inlet is about 10 mm off the central axis. Nevertheless, an axisymmetric computational model is chosen assuming that the off-distance has small influence on the overall flow and temperature distributions. This decision is motivated by the enormous reduction of computational costs compared to a three-dimensional computational model. A finite volume grid is generated consisting of 18 000 control volumes, 60 in radial, 300 in vertical direction distributed equally in each direction. Grid refinement studies show that the numerical solution does not change significantly in this range with increasing grid refinement.

1.3. Results on Thermofluidynamics and Process Uniformity

In fig. 2, numerical and experimental temperature recordings (obtained from thermo-couples-measurements [1]) are shown. The temperature increase applied to both simulation and experiment during compression is approximately 11.5 K for the upper curve (Thermocouple TC 13) and 10.5 K for the central curve (thermocouple TC 23). During compression, an excellent agreement between simulation and experiment can be observed for both thermocouples. This is valid also for the holding phase, apart from the deviation due the temperature increase induced by the additional compression cycles. Still the deviation remains below 1 K at the end of the holding phase after 1000 s.

The deviations are stronger for the lowest curve (thermocouple TC 31). Here, the numerical simulation underestimates the experiments by about 2K. Possible reasons for this are the asymmetry of the real geometry (inlet is 10 mm of the central axis) not accounted for in the simulation as well as the presence of the fixture of the thermocouples may disturb the local flow field.

Further information about the thermofluidynamics can be obtained from the field distributions shown in fig. 3. From left to right, velocity and temperature distributions can be observed shortly before (136 s) and shortly after the end of the compression (182 s), roughly in the middle (500 s) and at the end of the holding phase (820 s). The transient character of both distributions is well illustrated. An overall temperature increase of about 12 K can be observed.

At 136 s, the cool inflow stream goes almost straight through to the top with a slight widening of its cross section and thus decreasing velocity from 0.24 m/s at the entry to approximately 0.07 m/s close to its upper end. Due to its density, which is higher than that of the surrounding fluid, a thin downward directed layer flow is visible close to this stream, generating a large eddy at the bottom. The deviation of the temperature recordings of TC 31 and simulation data are probably related to the existence of this eddy. This flow pattern incorporates cool

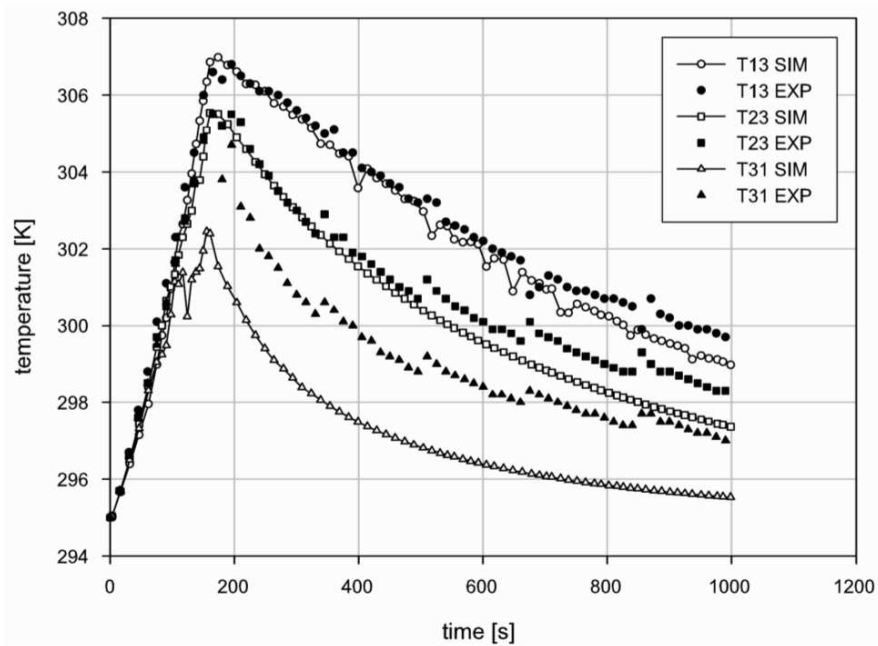


Fig. 2. Temperatures vs. time characteristics for 500 MPa target pressure.

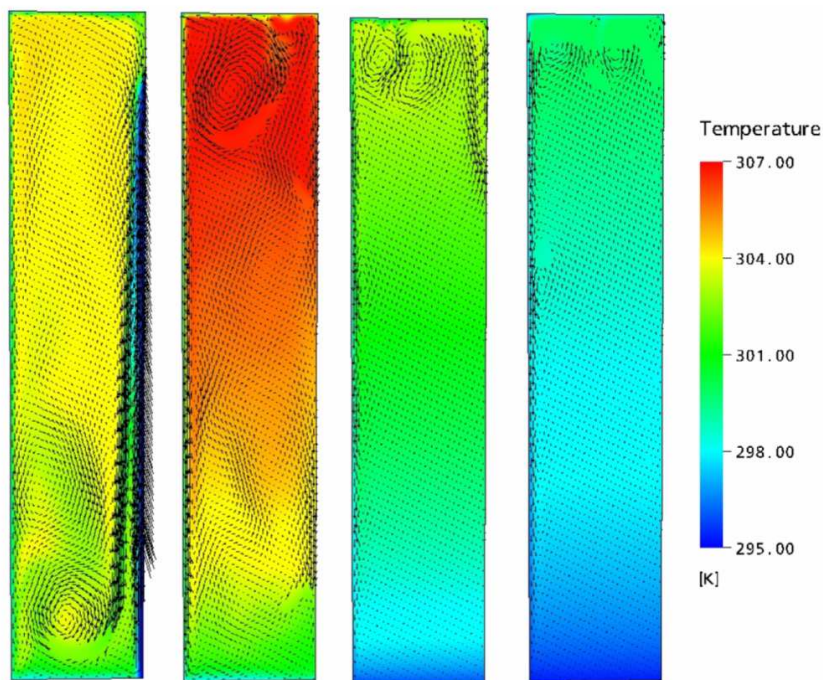


Fig. 3. Temperature and velocity distributions at 136, 182, 500 and 820 s (left to right) for process with 500 MPa final pressure.

fluid and is very stable during time evolution leading to relatively small numerical temperature increase in the region of TC 31. In the experiment [1], this axisymmetric eddy probably does not exist (unfortunately no possibility exists at present to confirm this), since the real configuration is not perfectly axisymmetric and, furthermore, at this location, the presence of the lower ring of the fixture will strongly affect the flow field.

For achievement of concise writing, the remaining states are discussed in brief. After the end of the compression phase, the momentum has been strongly redistributed. A large eddy develops on the top due to descending fluid previously cooled at the upper wall. Furthermore a downward directed boundary layer flow can be observed at the outer wall. During later states of the holding phase, an attenuation of fluid motion and ongoing compensation of temperature differences can be observed. At the end (i. e. at 820 s) a temperature difference of about 6 K to 7 K remains.

Three different cases are considered in order to investigate the degree of uniformity to be expected for different heat transfer conditions. The first case considers the real configuration as described above: i. e. the outer wall of the autoclave is tempered by a temper liquid. This implies a transient temperature distribution on the solid-liquid interface (the inner wall of the autoclave) as shown above. The second case assumes (hypothetical) adiabatic conditions, which can be realised by adding a layer of insulation material on the inner wall. The third case is again based on the real configuration, but viscosity is scaled by a factor of 100 assuming that the kinetics of inactivation remains unaffected as seen before in [9].

In fig. 4 the inactivation process of α -amylase in the solute mentioned above is shown for the three cases at 820 s. Note that individual legends are given for each case. In the standard case, the activity varies in a range between 37 and 55%, where the maximum activity retention exists in a region close to the inlet, and represents only a minor fraction of the total value. The adiabatic case exhibits a distribution in a comparably narrow range between 17 and 23%.

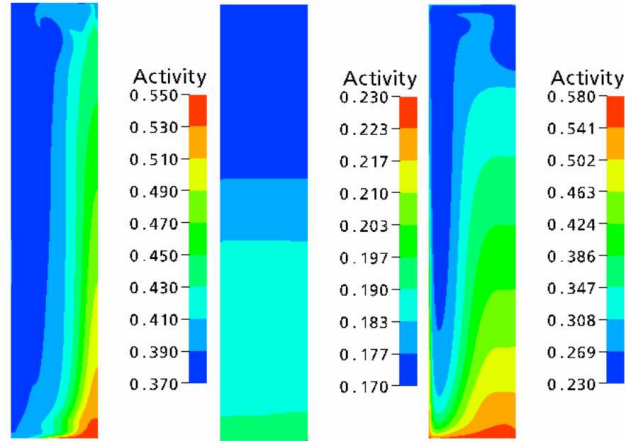


Fig. 4. Activity distribution for 500 MPa final pressure at 820 s. Pictures show standard case (left), adiabatic case (centre) and high viscosity case (right).

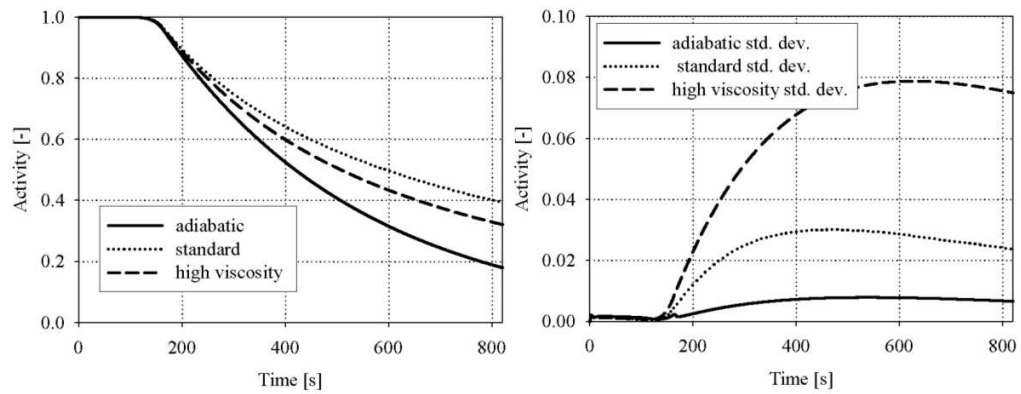


Fig. 5. Volume weighted average activity and standard deviation.

This difference is due to minor temperature heterogeneities induced by the inflow of fluid at a constant temperature of 313 K that mix with the warmer fluid in the chamber. Furthermore, due to the cumulative temperature effect, the overall level of activity retention is much lower than in the standard case, which is a desirable effect. Use of a higher viscous fluid considerably reduces the hydrodynamic compensation time scales that, in turn, facilitate the formation of process non-uniformities. This can be observed in the present activity distribution. Its range is between 23 and 58%. This is substantially larger than in the standard case and, of course, in the adiabatic case.

In fig. 5 the volume weighted average activity and its standard deviation vs. time are illustrated. The average value together with the standard deviation reflects the degree of non-uniformity of the process and enhances the information obtained from the field distribution. As can be seen from the left viewgraph of fig. 5, the average activity of the adiabatic case is more than twice as low as the standard case. If the average activity obtained for the standard case after 820 s (i. e. 40%) is defined as a target value, the process cycle of the adiabatic process could be shortened to approximately 500 s. This measure represents a tremendous reduction of the process cycle duration and thus an increase of economic efficiency.

The average activity for the high viscosity case is lower than that of the standard case, which seems surprising at first glance. A closer look at the involved effects reveals that the

conduction-dominated heat transfer maintains a high temperature in a large part of the vessel, inducing a comparatively rapid inactivation there. In the centre, where cold substrate enters into the domain, the inactivation is less efficient, as can be seen from the field distribution. However, the occupied volume fraction is considerably smaller. The standard deviation of the volume weighted average is considered as a measure of the non-uniformity of this process. It is depicted in the right part of fig. 5. In all three cases it can be observed that both reduction of the average activity and increase of the standard deviation become most prominent at the beginning of the holding phase, when the pressure is built up completely and temperature heterogeneities become apparent. The adiabatic process can be identified as the one leading to the smallest degree of non-uniformity. The standard deviation is non-zero because cold fluid enters the domain during the compression and mixes slowly with the warmer fluid inside, which induces small heterogeneities in the activity distribution (see fig. 5). Its maximum is reached at 550 s. A slight decrease can be observed until the end of the process. In the standard case, the maximum appears at 400 s. The following decrease is stronger than in the previous case, which is related to the intensive convective transport (large hydrodynamic compensation time scale) leading to a reduction of spatial heterogeneities. The high viscosity case has its maximum at 600 s, thus considerably later, and reduces only slightly until the end of the process. Compared to the standard case, convective transport is reduced (hydrodynamic compensation time scale is hundred times smaller). Thermal and activity heterogeneities can build up during a large part of the process cycle before free convection starts to attenuate the gradients. At the end of the process, the standard case yields an activity retention of $39.3 \pm 2.37\%$, the adiabatic case yields $18 \pm 0.66\%$ and the high viscosity case yields $32.1 \pm 7.5\%$.

1.4. Conclusions on Thermofluidynamics and Process Uniformity

In order to assess the process uniformity of a representative high pressure process, an enzyme inactivation of *Bacillus subtilis* α -amylase dissolved in a 0.01 M Tris HCl buffer (pH 8.6) at a concentration of 15 g per litre is simulated. The activity retention is obtained as transient field distribution. From various parameter studies, it can be shown that the thermal insulation of the inner wall of the chamber leads to a minimisation of the process non-uniformity. Furthermore, the process cycle can be reduced by 40% if the activity retention of the standard (non-zero heat transfer) process is defined as a target value. The use of higher viscous fluids leads to a substantial increase in the non-uniformity of 23.4% of the average value, whereas the average reduces slightly compared to the standard case. Here again, measures to assure (almost) non-zero heat transfer would lead to an inactivation result with minimum non-uniformity. Finally, one can conclude that thermal insulation of the inner wall of the high pressure chamber is the key to both a high degree of uniformity and efficient process cycles. Technical feasibility has to be analysed in a next step of investigation.

2. Micro-Biomechanics in High Pressure Processing

High pressure induced inactivation of micro-organisms is investigated intensively. This is done almost exclusively on a molecular level, but little is known about the mechanical effects on living cells and the resulting morphological changes [15].

Morphological changes of yeast cells (*Saccharomyces cerevisiae*) under high hydrostatic pressure with damage of cell organelles prior to cell wall disruption at pressure levels between

400 and 500 MPa are reported in [16]. The analysis is carried out ex-situ, since in-situ observation of cells exposed to high hydrostatic pressure is possible only at moderately high pressures. Moreover, an in-situ observation of cell organelles seems even to be impossible at present. Therefore, the present contribution intends to deliver a mathematical model and a simulation of the mechanical effects during the high hydrostatic pressure treatment of *Saccharomyces cerevisiae* (baker's yeast). This organism is chosen, because it is widely used in food and biotechnology. Furthermore, the organism is of a certain mechanical complexity since it has a cell wall as well as a membrane and organelles.

The structure of a Baker's yeast cell (*Saccharomyces cerevisiae*) is shown in fig. 6. It has an ellipsoidal form with a characteristic length of 5 to 10 μm . The cell is bounded by a cell wall consisting of a strongly cross linked network of polysaccharide chains giving the whole cell wall the properties of a single macro-molecule. The cell wall material is referred to as murein. It is a porous structure and allows the transfer of water molecules and ions. The cell wall has a bud scar, which is generated during the diploid budding of a daughter cell.

The cell membrane is bounding the cytoplasm inside the cell and regulates the transfer of water and ions. It is attached to the inner surface of the cell wall and consists of a lipid double layer that is fluid in its native state. Functional protein molecules integrated in the membrane are providing the transport and keep up the trans-cellular gradients. The cell is filled with cytoplasm, which is a watery solution of enzymes, proteins and ions. Furthermore, different cell organelles are suspended in the cytoplasm, from which the most important one is the nucleus containing the DNA. Furthermore, a vacuole serving as reservoir of water, lipids or gas is one of the dominant internal parts of the cell besides mitochondria and the endoplasmic reticulum.

The process to be considered is the application of high hydrostatic pressure to a yeast cell suspended in a liquid medium transferring the pressure ideally to the outer cell wall. It is supposed that the considered single cell is freely suspended in a liquid, such that a constant pressure acts on every point of the cell wall. Motion of the pressure transferring liquid as well as thermal effects due to transfer of external work to internal energy are not taken into account at present. The pressure is increased from ambient pressure up to a maximum value of $p_{\text{max}} = 500 \text{ MPa}$ within a process time $t_p = 50 \text{ s}$. While in reality, the pressure is conserved for several minutes in order to obtain the desired pressure induced effects, in the present case only the compression phase is accounted for. The phase of constant pressure load is stationary and mechanically identical to that obtained at the end of the compression phase and, therefore,

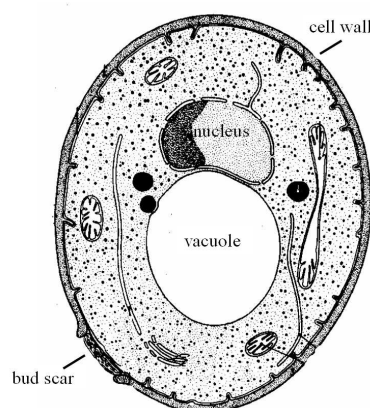


Fig. 6. Structure of Baker's Yeast.

does not need further consideration in the present context.

2.1. Model Definition

In order to describe the mechanical behavior of the cell, the complex structure of the cell is reduced to an axis-symmetric model containing the relevant structural parts of the cell: the cell wall, the cytoplasm (contained in the cell), the nucleus and the vacuole. Other cell organelles are supposed to be of minor importance for the mechanical behavior of the cell. Membranes around the whole cell, the nucleus and the vacuole are taken into account as material surfaces. The geometrical shape of the yeast cell model represents a cross section through an ellipsoid with an imperfection at the bottom representing the bud scar. It contains a spherical nucleus and a spherical vacuole placed along the axis of symmetry at distinct locations. The radius of the nucleus has been chosen arbitrarily as a characteristic length $L = 1 \mu\text{m}$. The maximum length of the cell is chosen to be equal to $10L$, the radius of the vacuole is $2L$, and the thickness of the cell wall is, apart from the bud scar, $0.2L$ [14]. A cylinder-coordinate system is defined as indicated in fig. 7 to describe the field distribution functions. Furthermore, a finite element mesh is illustrated, which will be commented on in a subsequent section.

2.2. Theoretical Considerations and Governing Equations

The fundamental equation for the description of the mechanical behaviour of the yeast cell during a high pressure treatment is Cauchy's equation of motion for a continuous medium

$$\rho \ddot{\vec{u}} = \nabla \cdot \Pi + \vec{k}, \quad (13)$$

where ρ is the density of the medium and the vector \vec{u} represents the displacement. The stress tensor is denoted by Π , ∇ represents the gradient operator and the vector \vec{k} a volume force. Due to the assumption of axis-symmetric conditions, the circumferential components of \vec{u} become zero as well as the variation of any quantity in the circumferential direction. The pressure $p_0(t)$ acts on the outer surface of the yeast cell following directly the operating pressure characteristics described in the previous section.

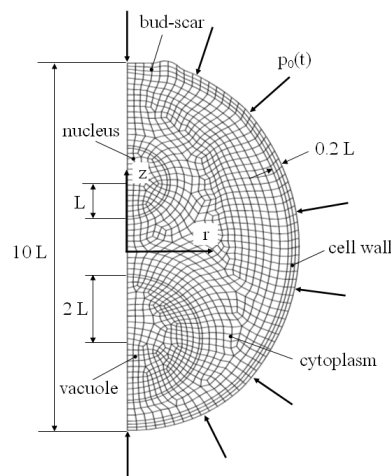


Fig. 7. Geometry of the model.

In order to get insight in the physical scales of the problem, a dimensional analysis of the Cauchy equation of motion is carried out. The coordinates and the vector of displacement are scaled with the typical length of the cell $L = 1 \mu\text{m}$, the time is scaled with the compression time $t_p = 50\text{s}$ (implying a compression rate of 10MPa/s), the density with the density at ambient conditions $\rho = 998\text{kg/m}^3$ and the stress tensor is scaled with the maximum applied pressure $p_m = 500\text{MPa}$. Furthermore, the volume force vector \vec{k} is assumed to be equal to $\rho\vec{k}$ leaving other forces (e. g. electro-static) out of consideration. From this the following equation is obtained:

$$\rho^+ \ddot{u}^+ + \frac{\rho_0 L^2}{p_m t_p^2} = \nabla^+ \cdot \Pi^+ + \frac{\rho_0 g L}{p_m} \rho^+ \vec{e}_g. \quad (14)$$

The superscript $+$ indicates dimensionless quantities and the vector \vec{e}_g is the unit vector in the direction of the gravitation. The coefficient of the acceleration term is of the order of magnitude of 10^{-20} , and the coefficient of the gravitation term is of the order of magnitude of 10^{-11} , while all other terms are of the order of magnitude of 10^0 . From this analysis two conclusions can be drawn. The first one is that the gravitational force has no major influence on the mechanical behaviour of the suspended cell. The second one implies that the inner time scale of the cell compared to the compression time scale is very small. Consequently, inertia effects can be neglected for this load case. The magnitude of the involved physical scales implies that the mathematical formulation reduces to

$$\nabla^+ \cdot \Pi^+ = 0. \quad (15)$$

Since mechanical properties of the individual organelles of the yeast cell are difficult to determine, the current model accounts for simplified material properties of the cytoplasm (a gel filling the voids inside the cell), a fat-containing vacuole and the cell wall. The mechanical properties of the cell wall are taken from [17], where the bulk modulus of the cell wall material is determined as $K_{cw} = 150 \pm 15\text{MPa}$ assuming almost incompressible, linear elastic behavior. Analysis of current model parameters as well as physical properties of cytoplasm suggests that the mechanical properties of cytoplasm exposed to high pressure can be approximated with those of pure water. Therefore, bulk modulus of water is derived from an equation of state valid under high pressure and is shown to depend linearly on pressure. Analogously, bulk modulus for the lipid contained in the vacuole is determined from published thermodynamic data. The governing equations are solved with finite element methods.

We use 1322 axis-symmetric 8-node-solid-elements in the whole computational domain. The pressure load is applied incrementally in order to achieve converged solutions at 10 load steps. Successive refinement of the computational mesh did not significantly influence the results.

2.3. Results on Micro-Biomechanics in High Pressure Processing

Our simulation results are compared to experimentally determined volume reduction at pressures up to 250MPa published in [18]. Generally, it can be stated that the data exhibit a good overall agreement, where the maximum deviation does not exceed 6% . This is most probably related to the fact that experimental volume measurements are based on the assumption that the cells have a spherical shape. Application of a pressure load of 400MPa generates a strong deformation of the initially spherical vacuole and nucleus (fig. 8). The overall shape of the cell approaches a spherical shape. The inner part of the cell remains in a hydrostatic stress state with zero von-Mises stresses. The maximum von-Mises-stress is located in the cell wall around $z = 0$ (coordinated system see fig. 7) and adopts values of up to 64MPa .

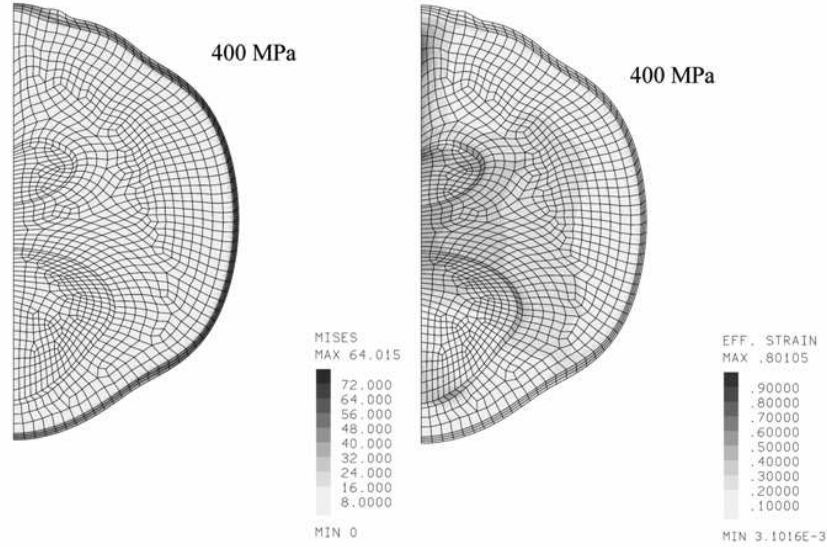


Fig. 8. Von-Mises-stress field and effective strain distribution.

The authors of [16] observe ex-situ that the membranes of the organelles are all disrupted after a high pressure treatment at 400 MPa at ambient temperature. The outer shape of the organisms remains unaffected in this case. The present contribution reveals that at any pressure level maximum effective strain values are located in the membranes of the organelles. According to the observations in [17] an estimate of the critical effective strain of $\epsilon_{VM,f} = 0.8$ upon failure of the organelle membranes can be delivered from the present load case at 400 MPa. Ex-situ investigations of yeast cells treated at pressures of 400 and 500 MPa [16], and critical values of the von-Mises stress upon failure for the cell wall material [17] at ambient non-hydrostatic conditions can be correlated to the results of the present analysis. The authors of [16] observe disruption of the cell wall at pressures above 400 MPa, while a von-Mises stress for failure of the cell wall is given in a range of $\sigma_{VM,f} = 70 \pm 4$ MPa [17]. Fig. 8 shows a maximum von-Mises stress of 64 MPa in a 400 MPa load case being slightly below this critical range. Latter is completely covered at a pressure load between 415 and 440 MPa.

In addition to that, it can be concluded from the dimensional analysis of the mechanical problem, that transient pressure application cycles in a high hydrostatic pressure process do not generate any dynamic response of the cell. Structural inactivation of the cells (e. g. damage of the cell wall or membranes) is a result of static load on the cell and can not be enhanced by transient pressure application. The latter has to be expected if the coefficient of the inertia term of the non-dimensional equation of motion takes on values of the order of magnitude of one. Thus, from

$$\frac{\rho_0 L^2}{p_m t_p^2} \approx 1 \quad \text{follows} \quad t_p = L \cdot \sqrt{\frac{\rho_0}{p_m}} \approx 1.41 \cdot 10^{-9} \text{ s}$$

corresponding to a frequency of approximately $f = t_p^{-1} = 700$ MHz. This value is far beyond the range of current application in HHP processing. These theoretical considerations confirm the observations in [19], who experimentally assess the influence of compression and decompression rates on the kinetic of inactivation of *Listeria innocua* and find out, that the inactivation is independent from the compression and decompression rate.

2.4. Conclusions on Micro-Biomechanics in High Pressure Processing

Referring to the questions formulated in the introduction following conclusions can be drawn: The interior of the cell is exposed to hydrostatic stress conditions as long as the material properties of the organelles do not differ much from those of the cytoplasm. The cell organelle membranes are strongly deformed prior to any damage of the cell wall. Pressure loads between 415 and 460 MPa induce mechanical cell wall damage. Compared to constant pressure application, transient pressure protocols in HHP processing do not enhance the mechanical action on the yeast cells. A dynamic response of the cells can only be expected at pressure oscillation frequencies superior to 700 MHz.

References

- [1] HARTMANN C., SCHUHHOLZ J. P., KITSUBUN P. ET AL. Experimental and Numerical Analysis of the Thermofluidynamics in a High-Pressure-Autoclave // *Innovative Food Science and Emerging Technology*. 2004. (in press).
- [2] HARTMANN C., DELGADO A. Convective and diffusive transport effects in a high pressure induced inactivation process of packed food // *J. of Food Eng.* 2003. Vol. 59, N 1. P. 33–44.
- [3] PEHL M., DELGADO A. Experimental investigation on thermofluidodynamical processes in pressurized substances // *Trends in High Pressure Bioscience and Biotechnology* (ed. R. Hayashi). Amsterdam: Elsevier, 2001. P. 429–435.
- [4] PEHL M., WERNER F., DELGADO A. First visualisation of temperature fields in liquids at high-pressure using thermochromic liquid crystals // *Experiments in Fluids*. 2000. Vol. 29, N 3. P. 302–304.
- [5] LUDI KHUYZE L., VAN DEN BROECK I., WEEMAES C.A. ET AL. Kinetics for isobaric isothermal inactivation of bacillus subtilis α -amylase // *Biotechnology Progress*. 1997. Vol. 13. P. 532–538.
- [6] DENYS S., VAN LOEY A.M., HENDRICKX M.E. A modelling approach for evaluating process uniformity during batch high hydrostatic pressure processing: combination of a numerical heat transfer model and enzyme inactivation kinetics // *Innovative Food Science and Emerging Technologies*. 2000. Vol. 1. P. 5–19.
- [7] HINRICHS J. Ultrahochdruckbehandlung von Lebensmitteln mit Schwerpunkt Milch und Milchprodukte – Phänomene, Kinetik und Methodik // Düsseldorf: VDI Fortschritt-Berichte Reihe. 2000. Vol. 3, N 656.
- [8] LUDI KHUYZE L., VAN DEN BROECK I., WEEMAES C.A., HENDRICKX M.E. Kinetic parameters for temperature pressure inactivation of bacillus subtilis α -amylase under dynamic conditions // *Biotechnology Progress*. 1997. Vol. 13. P. 617–623.
- [9] HARTMANN C., DELGADO A. Numerical simulation of convective and diffusive transport effects on a high-pressure-induced inactivation process // *Biotechnology and Bioengineering*. 2002. Vol. 79. P. 94–104.
- [10] SAUL A., WAGNER W. A fundamental equation for water covering the range from the melting line to 1273 K at pressures up to 25 000 MPa // *J. of Phys. and Chem. Reference Data*. 1989. Vol. 18. P. 1537–1564.

- [11] WATSON J.T.R., BASU R.S., SENEGERS J.V. An improved representative equation for the dynamic viscosity of water substance // J. of Physical and Chemical Reference Data. 1980. Vol. 9.
- [12] FÖRST P., WERNER F., DELGADO A. The viscosity of water at high-pressures-especially at subzero degrees centigrade // Rheologica Acta. 2000. Vol. 39. P. 566–573.
- [13] FÖRST P. In-situ Untersuchungen der Viskosität flüidier komprimierter Lebensmittel. München, 2001. 178 p.
- [14] SCHLEGEL H.G. Allgemeine Mikrobiologie. Stuttgart: Thieme, 1992.
- [15] HARTMANN C., DELGADO A. Numerical Simulation of the Mechanics of a Yeast Cell under High Hydrostatic Pressure // J. of Biomechanics. 2004. Vol. 37, N 7. P. 977–987.
- [16] SHIMADA S., ANDOU M., NAITO N. ET AL. Effects of hydrostatic pressure on the ultrastructure and leakage of internal substances in the yeast *Saccharomyces cerevisiae* // Applied Microbiology and Biotechnology. 1993. Vol. 40. P. 123–131.
- [17] SMITH A.E., MOXHAM K.E., MIDDELBERG A.P.J. Wall material properties of yeast cells. Pt II. Analysis // Chemical Engineering Science. 2000. Vol. 55. P. 2043–2053.
- [18] PERRIER-CORNET J.M., MARECHAL P.A., GERVAIS P. A new design intended to relate high pressure treatment to yeast cell mass transfer // J. of Biotechnology. 1995. Vol. 41. P. 49–58.
- [19] RADEMACHER B., WERNER F., PEHL M. Effect of the pressurizing ramp on the inactivation of *Listeria innocua* considering thermofluidodynamical processes // Innovative Food Science and Emerging Technologies. 2002. Vol. 3. P. 13–24.

Received for publication September 27, 2004